buildings

MDPI

Article

A Study on Seismic Dynamic Response of Pile-Supported Tunnels in Deep Backfill Area of Soil–Rock Mixture Based on a Model Test

Hanlin Li, Xiaoguang Jin *, Guodong Sun and Jie He

School of Civil Engineering, Chongqing University, Chongqing 400038, China; 20211601018@cqu.edu.cn (H.L.); 20191613025t@cqu.edu.cn (G.S.); 20201601069@cqu.edu.cn (J.H.)
* Correspondence: jinxiaoguang@cqu.edu.cn

Abstract: Aiming to address the problem of construction and environmental risks in tunnel construction through the soil–rock mixture backfill area, this paper carried out a seismic dynamic response model test of a pile-supported tunnel based on practical projects. Firstly, the stress–strain curves and failure characteristics of the soil–rock mixture in the study area were obtained through triaxial tests, and based on this, similar materials for the model test were developed. Then, a vibration table model test was devised to investigate the seismic dynamic response of the pile–tunnel structure. The findings revealed the following: when subjected to seismic waves, the soil–rock mixture stratum displayed a "skin effect" in its acceleration response, indicating that closer proximity to the surface led to heightened horizontal acceleration responses; the horizontal peak acceleration of the grouting mixture stratum in the vertical direction exhibited a "Zigzag" pattern; the peak values of strain response and bending moment in the tunnel lining cross-section exhibited an "X" shape and inverted "V" shape, respectively. The bending moment at the pile crown increased alongside the peak value of the input seismic wave acceleration. The maximum surface settlement in the model ranged from 0.5 to 1 cm, with the tunnel–pile structure effectively mitigating surface settlement.

Keywords: soil–rock mixture backfill area; pile-supported tunnel system; seismic dynamic response; physical model test

Citation: Li, H.; Jin, X.; Sun, G.; He, J. A Study on Seismic Dynamic Response of Pile-Supported Tunnels in Deep Backfill Area of Soil–Rock Mixture Based on a Model Test. *Buildings* **2024**, *14*, 791. https://doi.org/10.3390/buildings14030791

Academic Editors: Bingxiang Yuan, Rajai Zuheir Al-Rousan, Shaobo Chai, Yongqiang Zhou, Erdi Abi and Longlong Lv

Received: 7 January 2024
Revised: 6 February 2024
Accepted: 12 March 2024
Published: 14 March 2024

1. Introduction

Earthquakes, as the world's largest natural disaster, frequently result in varying degrees of damage to tunnels, such as cracking, collapsing, and displacement of the lining [1]. The shaking-table model test is the most direct method to study the seismic response of structure and the mechanism of earthquake damage [2,3]. The selected seismic wave is output to the shaker table to generate excitation to the shaker model structure through the control room, so that the seismic process can be reproduced relatively realistically. The seismic dynamic response of orthogonal tunnels has been a prominent focus of research in the past. Pai Lifang et al. [4] carried out shaking-table tests based on typical cases of cross-tunnel underpass landslides to reveal the regional spatial dynamic response characteristics of lining structures. Based on the interchange tunnel project, Lai Tianwen et al. [5] designed a large-scale shaking-table model test to study the seismic dynamic response characteristics of the orthogonal tunnel. At present, researchers are beginning to focus on the seismic dynamic response of parallel tunnels. Sun, TC et al. [6] carried out a model test of the portals of two parallel tunnels to learn about the dynamic response of tunnel liner and the interaction between surrounding rock and liner in earthquakes. Tao Yang et al. [7] investigated the dynamic response and the failure characteristics of a parallel overlapped tunnel under seismic forces by employing shaking-table tests. However, a pile-supported tunnel structure is a common form of tunnel construction, on which there is little shaking-table model test research.

The research of similar materials in tunnel shaking-table tests is also a focus, including those in tunnel lining and surrounding rock. Wu Honggang et al. [8] adopted hard PVC as the main material and applied a mixture of gypsum, quartz sand, and water as a 5 mm thick shell to complete the production of the lining model; D. K. Singh et al. [9] used different materials to simulate damaged and undamaged tunnels and studied the seismic performance of damaged tunnels in aftershocks. Hao Zhou [10] studied the seismic dynamic response of a large-section tunnel in compacted clay by filling a container with clay soil; Cho Mya Darli [11] carried out a series of shaking-table tests on the integrated corridor tunnel in the mixed stratum of sand and clay, and the results showed that the dynamic response of the tunnel was significantly different in the clay and sandy stratum. To study the dynamic response of special soil under tunnel shaking-table tests, most of the current studies applied site soil without considering the similarity relationship [12].

In the process of infrastructure construction in mountainous cities, a large number of soil–rock mixed backfills were formed due to site leveling; therefore, some lines inevitably pass through these soil–rock mixed backfill areas. Some other scholars have carried out research on the characteristics of soil–rock mixture (SRM). Simoni et al. [13] conducted triaxial tests on soil–rock mixtures to analyze the stress–strain relationship, and the results showed that such materials had obvious shear expansibility; Huang Wenjian et al. [14] and Cao Wengui et al. [15] used the orthogonal experimental design method to analyze the influence of various factors such as rock content on the physical and mechanical properties of SRM, among which rock content has the greatest influence on the shear strength; Xia Jiaguo et al. [16,17] studied the effects of rock content and confining pressure on the mechanical properties of SRM using a large triaxial shear instrument, the results showed that the stress–shear displacement curve had a "jump" phenomenon, and the shear index parameters first increased and then decreased with the increase in rock content, and always increased with the increase in confining pressure. The preceding research on soil–rock mixture characteristics enables the development of a SRM similar material that meets the similarity relationships and certain failure characteristics in the model test.

In this paper, based on the subway tunnel project in Chongqing, a small clear distance pile-supported tunnel model was made according to the similarity theory. Furthermore, SRM similar materials reflecting certain failure characteristics were developed based on triaxial tests. The study focuses on the seismic dynamic response of tunnel lining structure, and to determine the unfavorable parts of the tunnel–pile structure, which can provide reference for the design, construction, and maintenance of similar projects.

2. Project Overview

2.1. Research Site

The research site is located in the deep soil–rock mixed backfill area of Chongqing Rail Transit Line 10, with an overlying thickness ranging from 11.5 to 56.0 m. The most dangerous section is a three-line tunnel, and the minimum spacing is only 3 m. Given the poor tunnel conditions, a series of precautionary measures were implemented to ensure project safety, including: ① preliminary curtain grouting; ② installation of tunnel piles to bolster the tunnel infrastructure. The profile view is illustrated in Figure 1, while a representative cross-section is delineated in Figure 2.

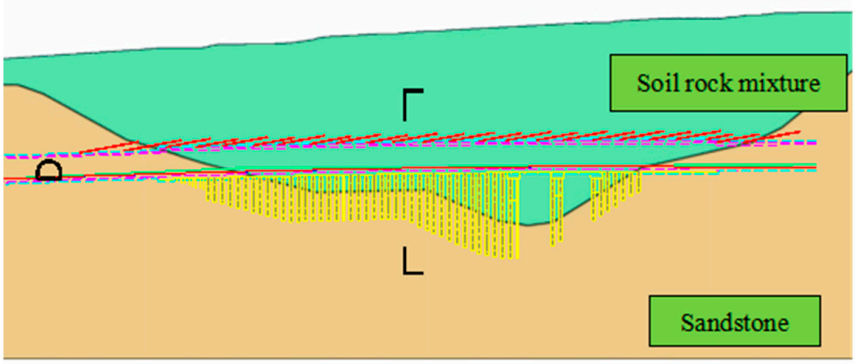

Figure 1. Profile view of the right line.

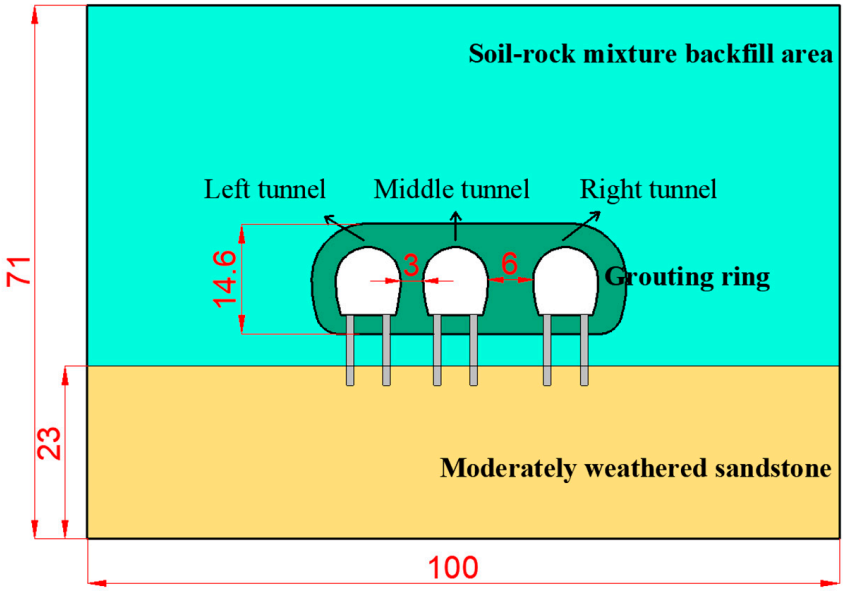

Figure 2. Cross-section of tunnel (unit: m).

2.2. Properties of Soil–Rock Mixture

First, the grading of the soil–rock mixture in the research site was measured, and its original gradation curve is depicted in Figure 3. Then, triaxial tests were conducted on the soil–rock mixture sample, and the stress–displacement curve was obtained as shown in Figure 4. It is worth noting that when there was no obvious mutation during the stress–displacement curve, the stress at 15% strain could be deemed as the failure value of the sample. The morphology of the post-failure samples is shown in Figure 5, showing a "drum shape". Utilizing nonlinear programming, the cohesion (c) was determined as 46.81 kPa, and the internal friction angle (φ) as 36.1° for the soil–rock mixture. The Mohr–Coulomb envelope is portrayed in Figure 6. According to geological investigation data and triaxial tests, the main mechanical properties of the prototype materials involved in this model test (soil–rock mixture, grouting mixture, sandstone, lining, and pile) are shown in Table 1.

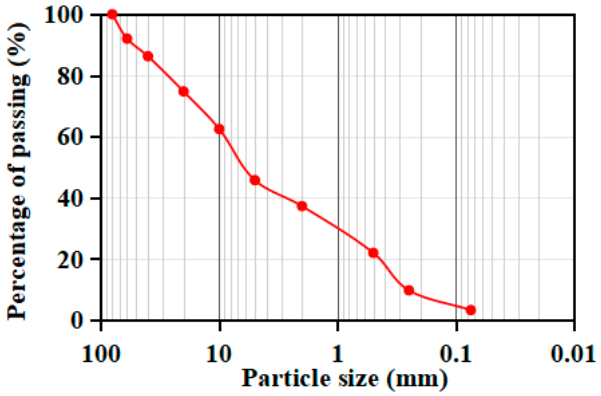

Figure 3. Gradation curve of SRM sample.

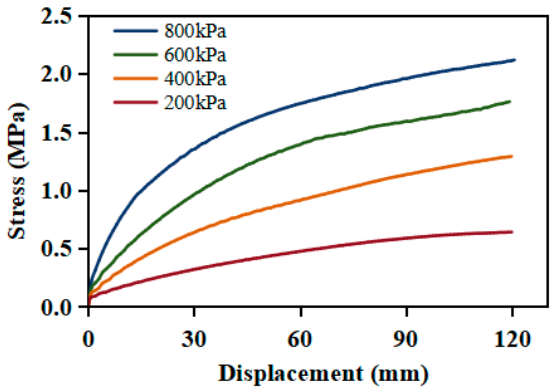

Figure 4. Stress–displacement curve of SRM sample.

(**a**) 200 kPa (**b**) 400 kPa (**c**) 600 kPa (**d**) 800 kPa

Figure 5. Failure mode of soil–rock mixture sample under different confining stress.

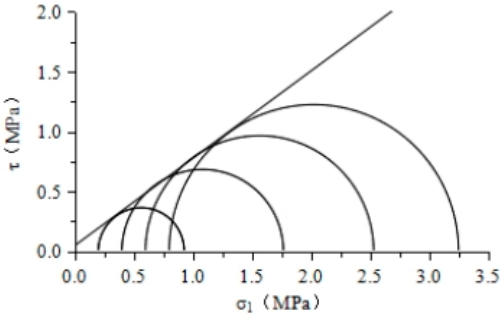

Figure 6. Molar envelope of soil–rock mixture sample.

Table 1. Mechanical properties of prototype materials.

Materials	c (kPa)	φ (°)	E (MPa)	Density (g/cm^3)	Poisson Ratio	Rock Content (%)	Uniaxial Compressive Strength (MPa)
SRM	46.8	36.1	64	1.8	0.3	40–60	
Grouting	400–800	35.8	140–280	2.0	0.28		
Sandstone	4000	41	5000	2.4	0.25		36.8
Lining			32,500	2.5	0.3		26.8
Pile			32,500	2.5	0.3		26.8

3. Design of the Model Test

3.1. Similar Materials

In the model test, the similarity between the model and the prototype should be ensured not only in the geometric scale, but also in the mechanical parameters. However, it is difficult to fully satisfy the similarity relationship between the model structure and the prototype structure, so priority was assigned to selecting key mechanical parameters impacting test outcomes and upholding their similarity in this experiment. Beyond the fundamental physical dimensions of length (l) and force (F), the design of the shaking-table model test must also incorporate the temporal factor (t) to maintain similarity ratios effectively.

In the dynamic model test, the inertia force of the structure is usually the primary load, and the relationship between the inertia force, damping force, and restoring force should be considered first in the study of dynamic problems. The dynamic equation is expressed as follows:

$$m(\ddot{x}(t) + \ddot{x}_g(t)) + c\dot{x}(t) + kx(t) = 0 \tag{1}$$

According to the requirements of equation analysis, the similar relationship of each physical quantity of the dynamic equation satisfies the equation:

$$S_m(S_{\ddot{x}} + S_{\ddot{x}_g}) + S_c S_{\dot{x}} + S_k S_x = 0 \tag{2}$$

Based on the similarity π theorem, applying dimensional analysis to the dynamic Equation (1), we obtain an expression with the fundamental similarity constants of elastic modulus E, density ρ, length l, and acceleration a:

$$S_\rho S_l^3 (S_\alpha + S_\alpha) + S_E \sqrt{\frac{S_l^3}{S_\alpha}} \sqrt{S_l S_\alpha} + S_E S_l^2 = 0 \tag{3}$$

$$\frac{S_E}{S_\rho S_\alpha S_l} = 1 \tag{4}$$

Based on the actual engineering and the dimensions of the model test table, the geometric similarity ratio was determined to be 1/80, considering geometric dimensions length l, density ρ, and acceleration a as the fundamental physical quantities. Subsequent parameters were analyzed using dimensional analysis to form similarity relationships, as shown in Table 2.

Table 2. Target parameters of similar materials.

Materials	c (kPa)	φ (°)	E (MPa)	Density (g/cm^3)	Poisson Ratio	Rock Content (%)	Uniaxial Compressive Strength (MPa)
Similarity relationship	$S_c = S_E$	$S_\varphi = 1$	$S_E = S_l S_\rho S_a$	$S_\gamma = S_\rho S_g$	$S_\varphi = 1$		Sucs = S_E
Similarity ratio	1/80	1	1/80	1	1		1/80
SRM	0.58	36.1	0.8	1.8	0.3	40–60	
Grouting	5–10	35.8	1.75–3.5	2.0	0.28		
Sandstone	50	41	62.5	2.4	0.25		0.46
Lining			406	2.5	0.3		0.33
Pile			406	2.5	0.3		0.33

(1) Soil–rock mixture and grouting mixture

In this paper, coarse quartz sand within 1~2 mm particle size and fine quartz sand within 0.5~1 mm particle size were used to simulate the coarse-grain phase in the prototype of soil–rock mixture, and fine sand within 0.1~0.2 mm particle size was used to simulate the fine-grain phase, and clay was selected as the cementing material. To maintain a rock content of 40% to 60% in similarity material, the mass ratio of coarse quartz sand and fine quartz sand needed to be controlled within the 40% to 60% range. Furthermore, the method of increasing the proportion of cementing material (clay) was used to simulate the grouting mixture. Through the above methods, three distinct samples were set, as shown in Table 3, and the configuration process is shown in Figure 7.

Table 3. Mix proportion design of similar materials.

Group	Main Ratio	Others	
	Coarse Quartz Sand (1~2 mm)–Fine Quartz Sand (1~2 mm)–Fine Sand–Clay	Water Content	Rock Content
Sample 1	2:2:5:1	7%	40%
Sample 2	2:2:4:2	10%	40%
Sample 3	2:3:3.5:1.5	10%	50%

(**a**) Stir (**b**) Standing (**c**) Package

Figure 7. Material preparation process.

Since the influence of groundwater was not considered in the actual project, unconsolidated and undrained triaxial tests were conducted to measure the mechanical parameters of similar materials. The stress–strain curves of the three samples subjected to confining stress of 50, 100, and 150 kPa are shown in Figure 8. By employing a nonlinear programming approach, the cohesion values (c) were determined as 0.8 kPa, 28 kPa, and 8 kPa for samples 1, 2, and 3, correspondingly, while the internal friction angles (ϕ) were calculated as 33.5°, 31°, and 38.5° for samples 1, 2, and 3. The corresponding Mohr–Coulomb envelopes are shown in Figure 9.

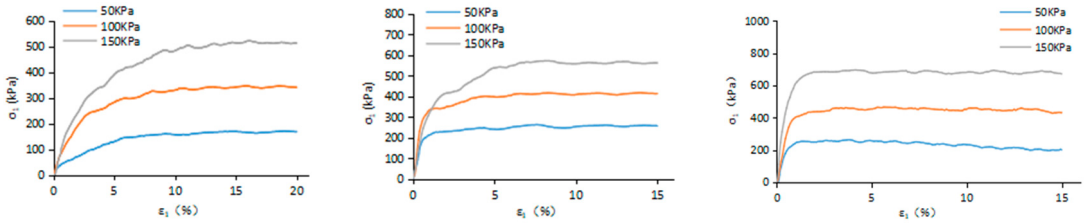

(**a**) Sample 1 (**b**) Sample 2 (**c**) Sample 3

Figure 8. Stress–strain curves of the samples.

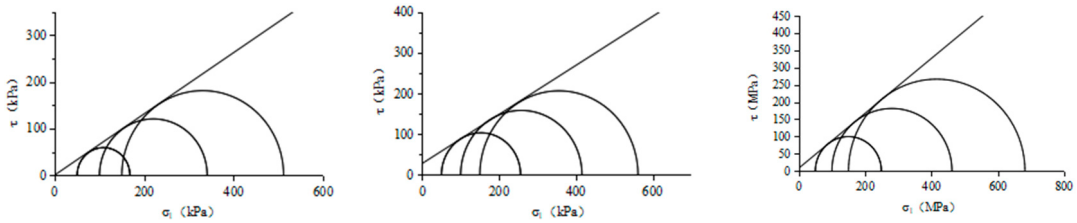

(**a**) Sample 1 (**b**) Sample 2 (**c**) Sample 3

Figure 9. Mohr–Coulomb envelopes of the samples.

Sample 1 was finally selected as the similar material of the soil–rock mixture, and sample 3 was selected as the similar material of grouting mixture. The failure mode of the sample is shown in Figure 10. It can be seen that the deformation of sample 1 under the triaxial compression test resembled a "drum shape", showing the same failure mode as that of the soil–rock mixture prototype. When subjected to a confining pressure of 50 kPa, sample 3 displayed an obvious 45-degree shear plane, and the failure mode was similar to the brittle failure of rock. When subjected to a confining pressure of 150 kPa, sample 3 did not exhibit obvious failure point, which was similar to the failure mode of soil. On the whole, sample 3 presented a failure mode similar to that of grouting mixture obtained by Hu [18].

50 kPa 100 kPa 150 kPa

(**a**) Sample 1

50 kPa 100 kPa 150 kPa

(**b**) Sample 3

Figure 10. Failure mode of sample 1 and sample 3.

(2) Lining and pile foundation

In this experiment, plexiglass was used to make the tunnel–pile structure. Flexural stiffness was adopted as the governing criterion for determining the thickness of the tunnel lining and the diameter of the tunnel pile. According to the principle of similarity ratio, the ratio between the flexural stiffness K of the actual tunnel lining and the flexural stiffness K_0 of the model test is $(1/80)^5$. Calculations revealed a tunnel lining thickness h_0 of 4 mm and a pile diameter D_0 of 6.2 mm. The completed model is shown in Figure 11.

Figure 11. Tunnel–pile structure model.

3.2. Test Scheme

(1) Model box design

A layered shear model box with a width of 0.85 m, a length of 0.95 m, and a height of 0.6 m was selected for the test. The model box was composed of multi-layer rectangular frames, each of which can move relative to the others in a certain amplitude, thus minimizing seismic wave reflection and offering a more accurate simulation of soil shear properties. Limited by the size of the shaking table, the original cross-section was simplified for the model test, as shown in Figure 12. The left and middle tunnels were selected as the research objects in the simplified section, and the tunnel spacing was adjusted to 52 mm in model box, retaining the characteristics of a tunnel with a small distance.

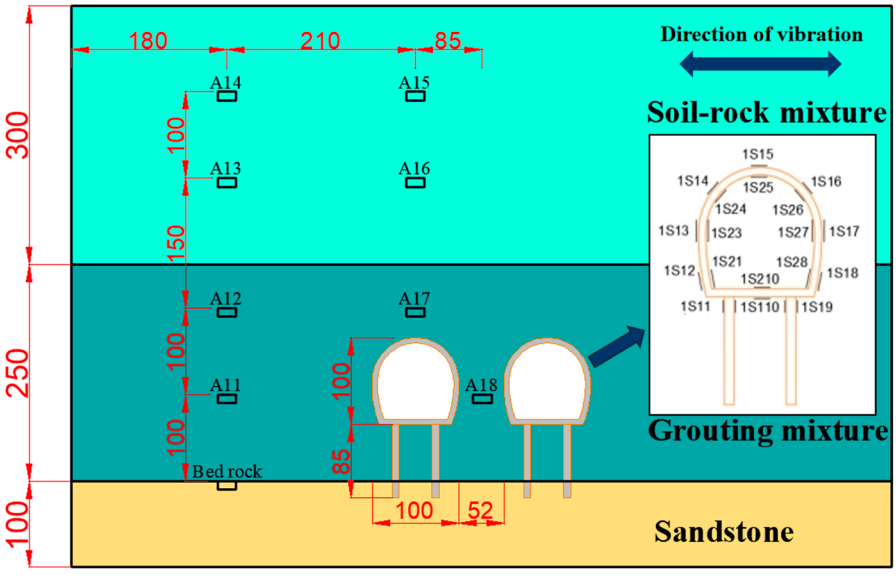

Figure 12. Simplified cross-section of the tunnel and layout of monitoring sensors (unit: mm).

(2) Sensor arrangement

In order to study the acceleration response characteristic of surrounding rock and tunnel–pile structure system, accelerometers and strain gauges were used in this experiment. The sensor layout of the model test is shown in Figure 12.

(3) Seismic wave selection

In this shaking-table model test, seismic waves were applied in the horizontal direction. Kobe wave, Wolong wave, and sine wave were selected as input signals. The original seismic wave exhibited significant displacements, sometimes exceeding 1 m, whereas the maximum displacement capacity of the shaking table was limited to 0.1 m. Hence, baseline adjustments were performed on the original seismic wave to ensure its displacement remained within the 0.1 m threshold. The time similarity constant was 1/10; consequently, the peak vibration time of Kobe and Wolong waves were compressed to 4 s, and that of the sine wave was compressed to 14 s.

The model filling process Is shown in Figure 13.

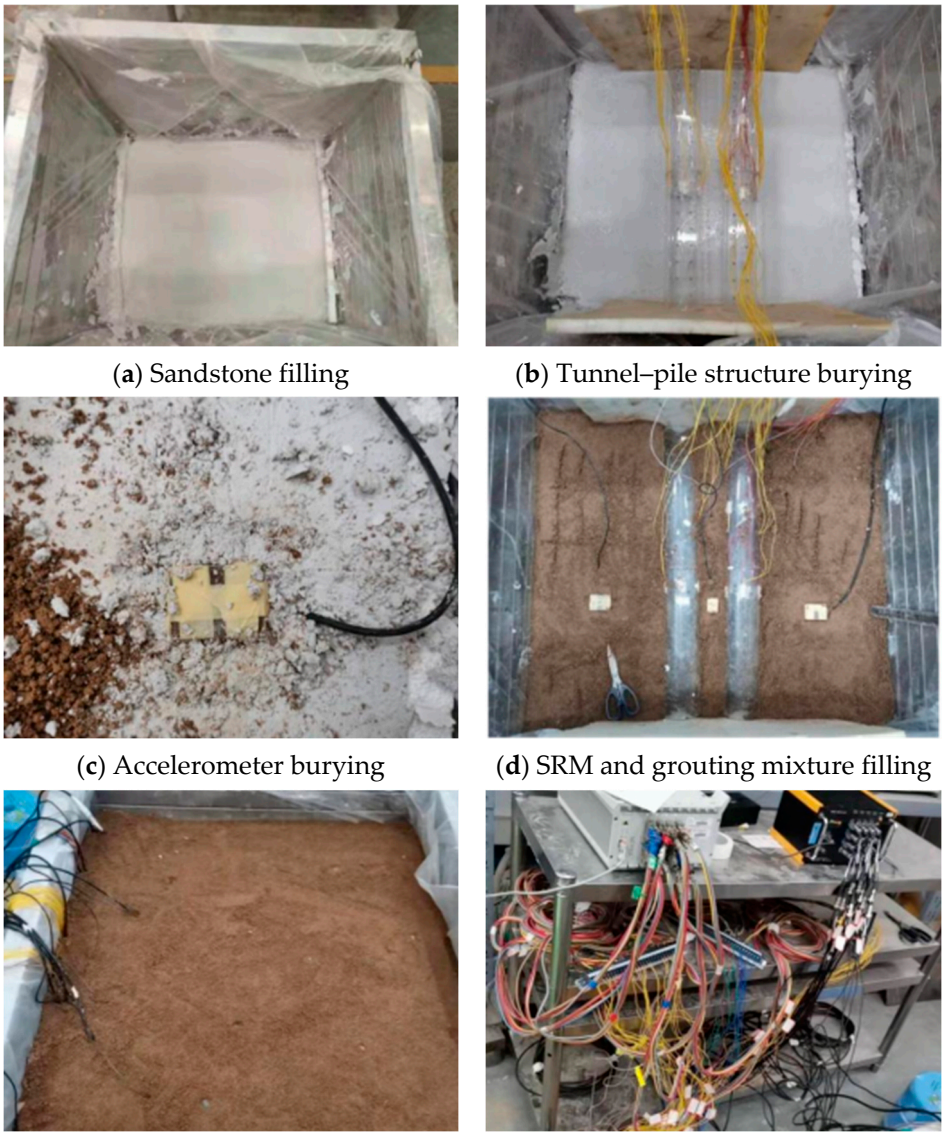

(**a**) Sandstone filling (**b**) Tunnel–pile structure burying

(**c**) Accelerometer burying (**d**) SRM and grouting mixture filling

(**e**) Model filling complete (**f**) Acquisition instrument

Figure 13. Model filling process.

4. Analysis of Test Results

4.1. Acceleration Response Characteristics of Surrounding Rock

After the model filling was completed, the boundary effect of the model was verified first. Kobe wave and Wolong wave with 1.2 g peak acceleration were the input. A comparison of acceleration–time history curves of measuring points A14 and A15 under the action of Kobe wave and Wolong wave is shown in Figure 14. The height of the curves was almost consistent, indicating that the boundary effect produced by the layered shear box in this test was small.

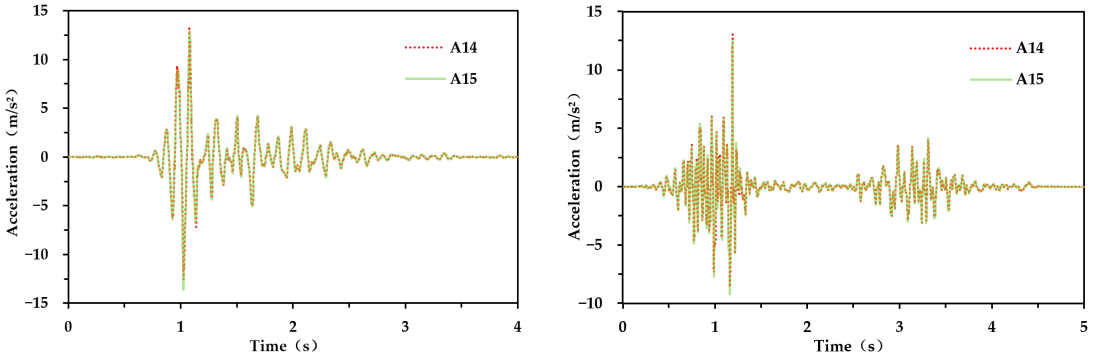

(**a**) Kobe wave (**b**) Wolong wave

Figure 14. Comparison of acceleration–time history curves of measuring points A14 and A15 under the action of Kobe wave and Wolong wave.

(1) Stratum acceleration response

As illustrated in Figure 12, five measuring points were arranged along the stratum height, sequentially identified from bottom to top as bedrock, A11, A12, A13, and A14. Figure 15 shows the curves of peak acceleration variation along the height of the stratum under different seismic waves. It can be seen that the peak acceleration within the stratum exhibited a consistent rise with increasing height from the base, distinctly displaying an amplification effect.

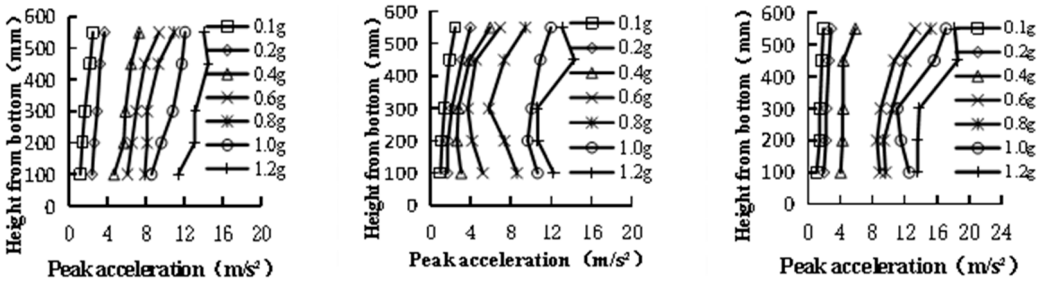

(**a**) Kobe wave (**b**) Wolong wave (**c**) Sine wave

Figure 15. Curves of peak acceleration variation along the height of the stratum under different seismic waves.

Under the action of Kobe wave, input seismic wave acceleration peak values ranging between 0.1 g and 1.0 g triggered a gradual increase in acceleration peak values along the stratum height, displaying a progressively intensifying trend suggestive of a pronounced "skin effect". However, as the input seismic wave acceleration peak value exceeded 1.0 g, the acceleration peak value decreased at the top of the SRM stratum (measuring points A14).

Conversely, under the action of Wolong wave and sine wave, the peak value of stratum acceleration at measuring points A11 and A12 showed a decreasing trend that strengthened

with higher input acceleration peak values. This attenuation is credited to the mitigation of stratum acceleration by the tunnel–pile structure when subjected to the Wolong wave and sine wave. However, when the peak acceleration of the input seismic wave exceeds 1.0 g, its peak value showed a "Z" shape along the stratum height, indicating a dual discernible shift in acceleration peak values with increasing distance from the base height.

To comprehensively study the acceleration amplification effect and variation law of the stratum, the peak acceleration ratio of individual points in relation to the peak acceleration at the surface of the platform was defined as the acceleration amplification coefficient for each point. Variation curves of acceleration amplification coefficient along vertical direction (bedrock, A11~A14) under different seismic waves are shown in Figure 16. It can be seen that within the soil–rock mixture layer (350~650 mm), when the input acceleration value remained below 0.2 g, the stratum's acceleration amplification coefficients increased monotonically along the vertical axis, indicating that the stratum response was in a linear stage at this time. As the peak input acceleration reached 0.4 g, a slight reduction in acceleration amplification coefficients occurred, yet the overall trend maintained a monotonic increase, indicating minimal soil damage. When the input acceleration peak value exceeded 1.0 g, the stratum acceleration amplification coefficients decreased significantly to less than one, indicating that the soil–rock mixture had entered a nonlinear reaction stage at this time. Potential plastic deformation within the stratum likely contributed to elevated damping and enhanced dissipation of seismic energy.

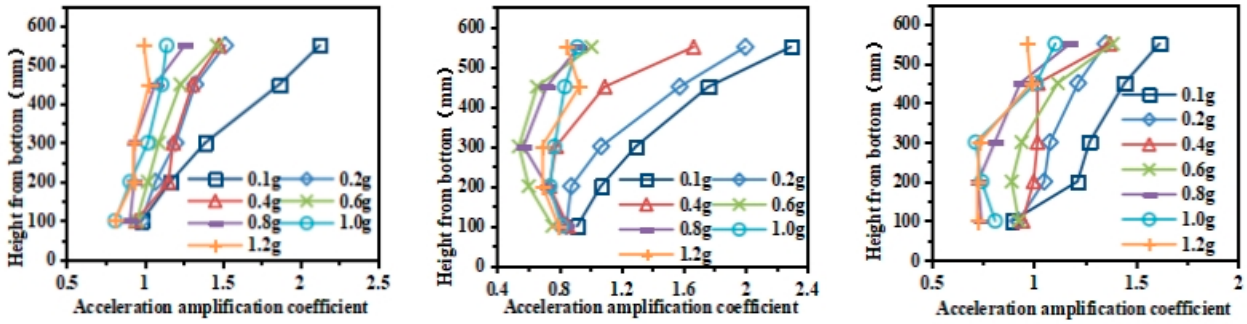

(**a**) Kobe wave (**b**) Wolong wave (**c**) Sine wave

Figure 16. Variation curves of acceleration amplification coefficient along height direction under different seismic waves.

(2) Influence of pile-supported tunnel structure on stratum acceleration

It can also be seen from Figure 16 that in the grouting stratum (100~350 mm), under the action of Wolong wave and sine wave, the acceleration amplification coefficient exhibited a transition from an increasing trend to a decreasing trend with rising input peak acceleration levels. This phenomenon is likely attributed to the emergence of the energy dissipation mechanism within the tunnel–pile system as the input peak acceleration intensified. This mechanism notably mitigated the stratum's acceleration response in this range. In addition, the cumulative damage caused by step-by-step seismic wave loading was also a part of the reason.

Under the action of different seismic waves, a comparison of peak acceleration values between points situated within the free field stratum (A12–A14) and points positioned above the tunnel axis (A15–A17) at equivalent elevations is presented in Figure 17. Across all three seismic wave scenarios, the peak acceleration of the measurement points above the tunnel axis was smaller than that of the free field stratum at the same height. When the input peak acceleration remained below 0.4 g, the difference between the two points was small; however, as the input peak acceleration exceeded 0.4 g, this difference showed a progressively increasing trend.

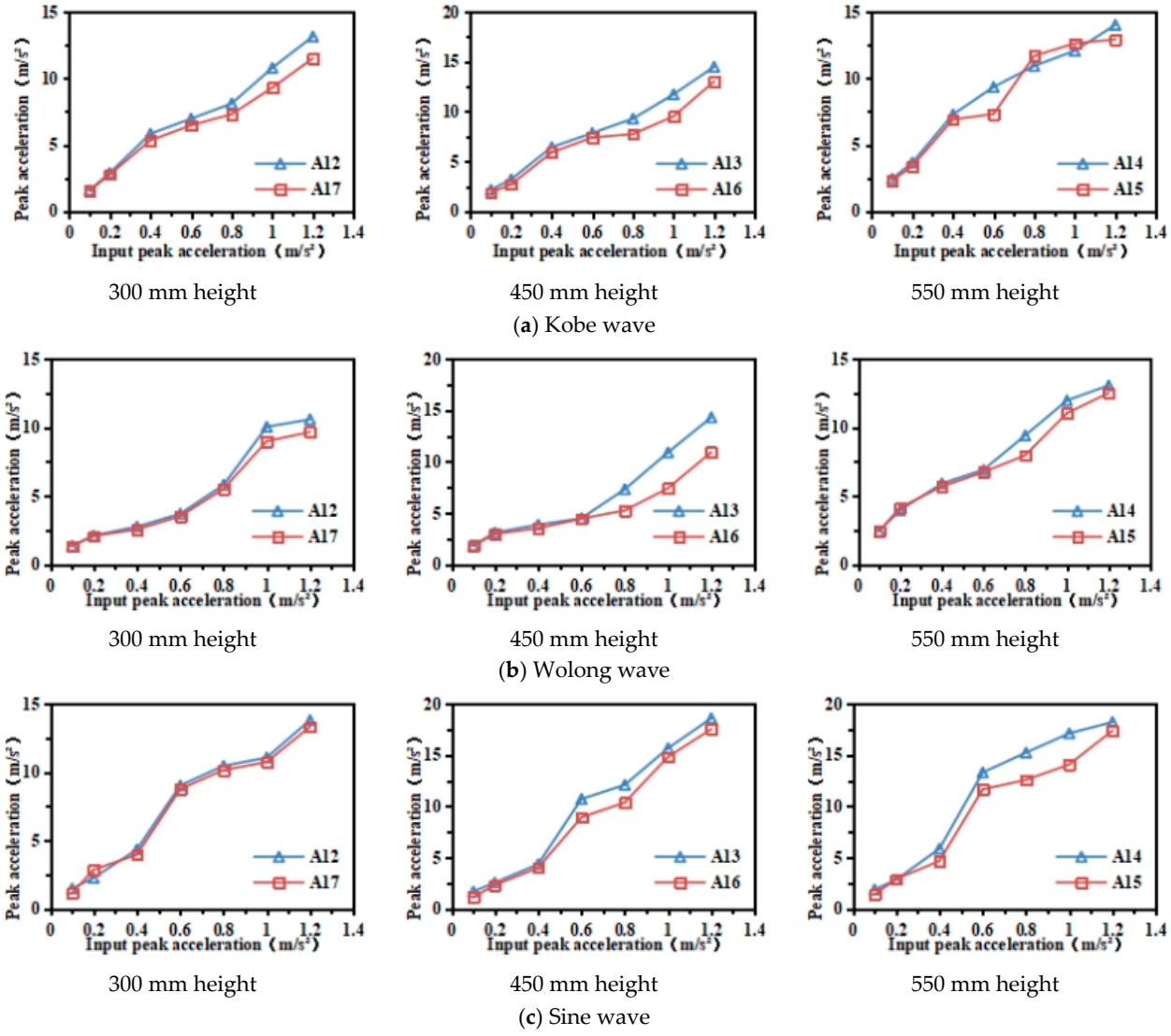

Figure 17. Comparison diagram of peak acceleration at different measuring points at the same height under the action of different seismic waves.

The relative difference percentage was defined as the ratio of the difference between the peak accelerations of two points at the same height to the peak acceleration of the free field stratum, as shown in Table 4. As can be seen from the table, the influence of the tunnel–pile system on stratum acceleration could reach up to 14.5%, and the greatest impact was located above the tunnel (at the height of 450 mm). There are two reasons why the tunnel–pile system had a weakening effect on stratum acceleration: first, the tunnel–pile system exerts a discernible energy dissipation effect on seismic waves; second, the settlement of the stratum above the tunnel was much smaller than that of the free field stratum, indicating the soil in the latter was comparatively looser and consequently led to higher acceleration values.

Table 4. Relative difference percentage of peak acceleration at different points at the same height.

Measuring Points	Height (mm)	Relative Difference Percentage of Peak Acceleration		
		Kobe Wave	Wolong Wave	Sine Wave
A14 A15	550	5.18%	4.07%	13.74%
A13 A16	450	12.61%	14.43%	13.08%
A12 A17	300	8.57%	5.81%	3.43%

4.2. Acceleration Response Characteristics of Pile-Supported Tunnel Structure

(1) Strain acceleration response of tunnel lining

The strain radar diagram of the tunnel lining under the action of Kobe wave, Wolong wave, and sine wave at different peak accelerations is shown in Figure 18. Analysis of the strain radar diagram reveals distinct patterns: On the outer edge of the lining, the highest strain peak occurs at the arch foot, followed by the arch shoulder, with comparatively lower values observed at the arch crown, arch waist, and inverted arch. The distribution of strain response peak value of the tunnel lining cross-section exhibited an "X" shape. On the inner edge of the lining, the peak value of strain at the left arch foot of the left tunnel lining was significantly greater than that at the right arch foot, indicating that the strain dynamic response of the inner edge of the lining was less pronounced than that of the outer edge due to the interaction of the two tunnels.

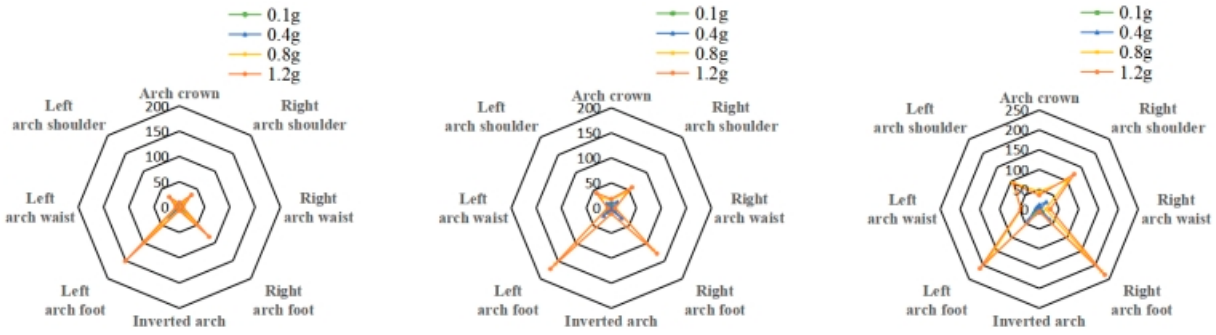

Kobe wave Wolong wave Sine wave

(**a**) Outer edge of the lining

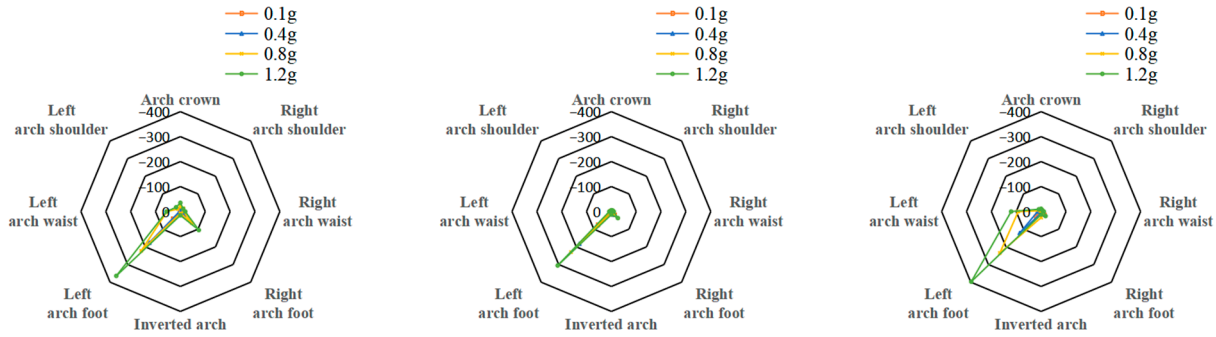

Kobe wave Wolong wave Sine wave

(**b**) Inner edge of the lining

Figure 18. Strain distribution on left tunnel cross-section under different seismic waves (unit: με).

(2) Bending moment acceleration response of tunnel lining

In order to study the bending moment value at each measuring point of the tunnel lining, the strain at the inner and outer edges of the lining was converted to the bending moment value according to Formula (5):

$$M = \frac{1}{2}(\sigma_1 - \sigma_2)W = \frac{1}{2}EW(\varepsilon_1 - \varepsilon_2) = \frac{1}{12}Ebh^2(\varepsilon_1 - \varepsilon_2) \quad (5)$$

where σ_1 and σ_2 are the stress on the inner and outer edges of the measuring point, ε_1 and ε_2 are the strain at the inner and outer edges of the measuring point, E is the elastic modulus of lining material, W is the resistance in cross-section, and b is the section width (1 m).

Under the action of three kinds of seismic waves, the maximum bending moment of each measuring point of the lining cross-section along the axis direction of the tunnel is

shown in Figure 19. The bending moment at the arch foot was the largest, followed by the left and right arch shoulder, and the bending moment at the inverted arch and arch waist was relatively small. The distribution of bending moment of the lining cross-section exhibited an inverted "V" shape on the whole. The bending moment increase effect at the right arch foot was smaller than that at the left arch foot, so its maximum bending moment value was 1/2–1/4 of the left arch foot.

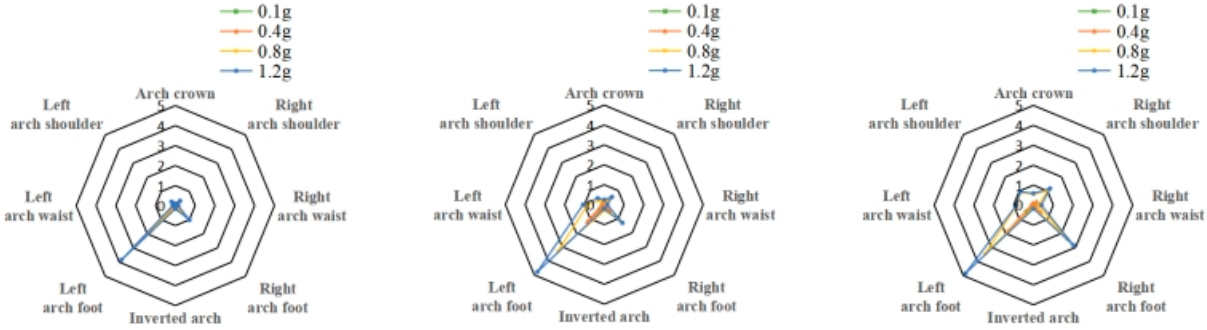

(**a**) Kobe wave (**b**) Wolong wave (**c**) Sine wave

Figure 19. Bending moment distribution of the left tunnel cross-section under different seismic waves (unit: N·m).

It can be seen from Figure 20 that with the increase in the input peak acceleration, the bending moment value at each position of the lining generally keeps increasing. When the input peak acceleration remained below 0.6 g, the bending moments of the lining retained a consistent increase trend except at the arch foot. As the input peak acceleration exceeds 0.6 g, the increase rate of bending moment slowed down at almost each position. As the input peak acceleration exceeds 0.8 g, the bending moment value of all lining positions did not increase except in the left arch foot.

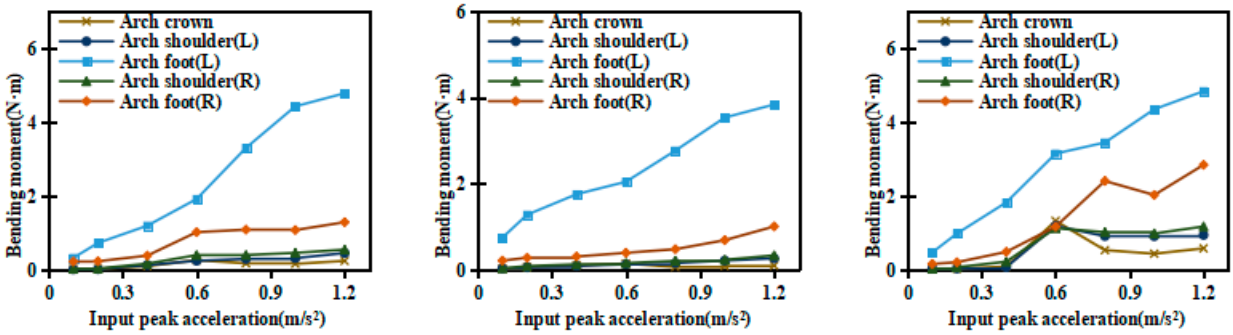

(**a**) Kobe wave (**b**) Wolong wave (**c**) Sine wave

Figure 20. Curves of the tunnel lining bending moment with input peak acceleration.

From Formula (5), the bending moment value at each position of the lining is positively correlated with the difference between the inner and outer strains. Moreover, the strain of the outer edge is positive, and the strain of the inner edge is negative, accentuating that bending moment distribution corresponds closely to higher absolute strain values. In this model test, the strain value at the left arch foot of inner edge is the largest, and the strain value at the right arch foot of outer edge is the second largest but much larger than that at other positions. Therefore, the bending moment of the lining cross-section is mainly affected by the left and right arch foot and exhibit an inverted "V" shape.

(3) Bending moment acceleration response of pile crown

Based on the strain data on the left and right sides of the pile crown, the bending moment changes of the pile crown under different seismic waves were plotted, as shown in Figure 21. Under the action of the three seismic waves, the bending moment of the left pile crown was greater than that of the right pile crown. Under the action of Kobe wave and sine wave, when the peak acceleration of input seismic wave was between 0.1–0.8 g, the bending moment of the pile crown increased gradually. As the peak acceleration of the input seismic wave exceeded 0.8 g, the bending moment of the pile crown approached stability or began to decline. The reason is that when the input peak acceleration exceeded 0.8 g, the grouting stratum besides pile entered large plastic deformation state; the peak dynamic earth pressure tended to be stable, so the dynamic bending moment also tended to be stable. When subjected to Kobe and sine waves, the decrease in the bending moment at the pile crown can be attributed to the energy dissipation after the grouting stratum reached the critical threshold of plastic deformation, causing a sudden decrease in dynamic earth pressure from the maximum value.

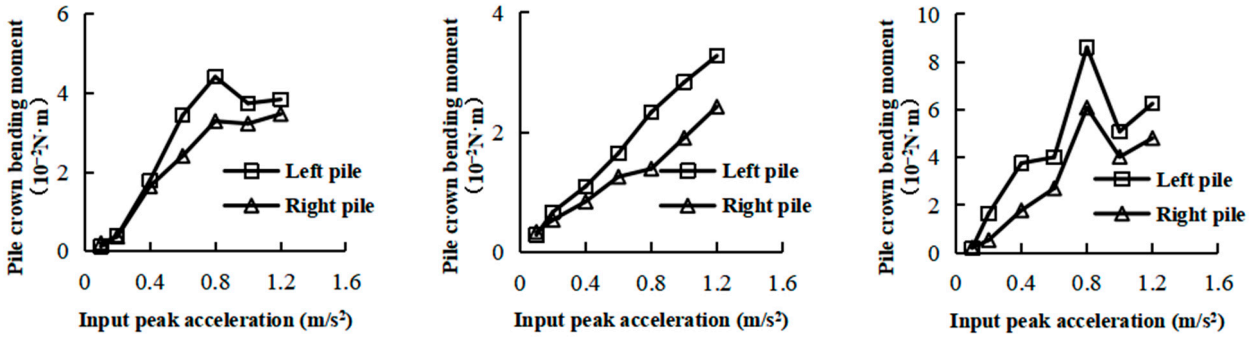

(**a**) Kobe wave (**b**) Wolong wave (**c**) Sine wave

Figure 21. Variation diagram of pile crown bending moment under different seismic waves.

4.3. Surface Settlement

After the shaking-table test was completed, the surface settlement was observed and measured. As shown in Figures 22 and 23, there was no significant settlement of the stratum above the tunnel. However, the free field stratum on both sides had obvious settlement. By measurement, the settlement amount on the left side reached 1 cm, and the right side reached 1.5 cm, indicating that the surface settlement of the soil–rock mixture was obvious under the action of the earthquake. However, the existence of a tunnel–pile structure mitigated the surface settlement obviously, and the uneven surface settlement would cause the cracking and destruction of above-ground roads and structures in practical engineering.

Figure 22. Surface settlement of the model.

Figure 23. Maximum surface settlement of the model.

5. Conclusions

In this paper, based on a subway tunnel project in Chongqing, the mechanical parameters of the soil–rock mixture at the original site of the project were measured based on a large-scale indoor triaxial test, and then the development methods and mechanical parameters of similar materials such as soil–rock mixture, grouting mixture, lining, and pile satisfying the similarity ratio were studied. Finally, the analysis was conducted from the stratum acceleration and its amplification factor, the distribution of strain and bending moment of the tunnel–pile structure, and the surface settlement. The main conclusions are as follows:

(1) Under the action of seismic waves, the acceleration response of soil–rock mixture stratum exhibited obvious "skin effect", indicating that closer proximity to the surface led to heightened horizontal acceleration responses; however, with the increase in the peak value of input seismic waves, the plastic deformation occurred in the upper stratum of the soil–rock mixture; the grouting stratum was obviously affected by the tunnel–pile structure, and the horizontal peak acceleration of the stratum in the vertical direction changes in a "Z" shape.

(2) The tunnel–pile structure had a weakening effect on the horizontal acceleration of both the stratum in its height range and the stratum above the tunnel.

(3) Under the action of seismic waves, the peak strain values at the arch shoulder and arch foot of the tunnel were larger, and the peak strain response of the tunnel lining cross-section generally exhibited an "X" shape. In the direction of the tunnel axis, the bending moment at the arch foot was the largest, followed by the left and right arch shoulder, and the bending moment at the inverted arch and arch waist were smaller. The bending moment of the lining cross-section exhibited an inverted "V" shape.

(4) The bending moment of the pile crown generally increased with the increase in the peak acceleration of the input seismic wave. When the peak acceleration of the input seismic wave exceeded 0.8 g, the increasing trend of the pile crown bending moment decreased.

(5) The maximum surface settlement in the model test was 0.5~1 cm, and the tunnel–pile structure effectively reduced the surface settlement but lead to uneven surface settlement.

Author Contributions: Conceptualization: X.J.; methodology, H.L. and G.S.; data processing, J.H.; writing—original draft preparation, H.L.; writing—review and editing, X.J.; project administration, X.J. All authors have read and agreed to the published version of the manuscript.

Funding: This research was funded by the Science and Technology Project of the Fifth Engineering Co., Ltd., China Railway 21st First Bureau Group (21J5GS-CQGD-JF-2020-003).

Data Availability Statement: The data presented in this study are available in the article.

Conflicts of Interest: The authors declare that this study received funding from the Science and Technology Project of the Fifth Engineering Co., Ltd., China Railway 21st First Bureau Group. The funder had the following involvement with the study: provides background information of the project (including geological data and design data).

References

1. Lai, J.; He, S.; Qiu, J.; Chen, J.; Wang, L.; Wang, K. Characteristics of seismic disasters and aseismic measures of tunnels in Wenchuan earthquake. *Environ. Earth Sci.* **2017**, *76*, 94. [CrossRef]
2. Zhang, F. Analysis of Dynamic Response of Subway Underground Structure Under Seismic and Second Development of Software. Master's Thesis, Huazhong University of Science & Technology, Wuhan, China, 2014. [CrossRef]
3. Thoms, R.; Kuesel, F. Earthquake design criteria for subways. *J. Struct. Div. Proc. Am. Soc. Civ. Eng.* **1969**, *95*, 1225–1328.
4. Pai, L.; Wu, H. Experimental study on dynamic response of tunnel lining structure orthogonal under-crossing a landslide under earthquake. *J. Rock Mech. Geotech. Eng.* **2022**, *41*, 979–994.
5. Lai, T.; Lei, H.; Wu, H. Vibration Acceleration Responses of Crossing Tunnels of Highway and Railway under Different Directions of Seismic Loads. *China Railw. Sci.* **2021**, *42*, 95–104.
6. Sun, T.; Yue, Z.; Gao, B.; Li, Q.; Zhang, Y. Model test study on the dynamic response of the portal section of two parallel tunnels in a seismically active area. *Water Energy Int.* **2011**, *68*, 74. [CrossRef]
7. Yang, T.; Rao, Y.; Wu, H.; Zhang, J.; Lei, H.; Ding, H. Dynamic Response of Parallel Overlapped Tunnel under Seismic Loading by Shaking Table Tests. *Shock Vib.* **2021**, *2021*, 2535762. [CrossRef]
8. Wu, H.; Pai, L.; Pang, W.; He, C.; Zhang, X.; Li, D. Vibration table tests on the acceleration response of a three-dimensional cross tunnel with small net spacing and small angle. *J. Vib. Shock* **2021**, *40*, 298–306. [CrossRef]
9. Singh, D.K.; Mandal, A.; Karumanchi, S.R.; Murmu, A.; Sivakumar, N. Seismic behaviour of damaged tunnel during aftershock. *Eng. Fail. Anal.* **2018**, *93*, 44–54. [CrossRef]
10. Zhou, H.; Wang, X.; He, C.; Huang, C.; Aenlle, M.L. Seismic Response of a Tunnel Embedded in Compacted Clay through Large-Scale Shake Table Testing. *Shock Vib.* **2018**, *2018*, 5968431. [CrossRef]
11. Mya, D.C.; Tang, A.; Huang, D.; Zhang, J. Large scale shaking table model test and analysis on seismic response of utility tunnel in non-homogeneous soil. *Earthq. Eng. Eng. Vib.* **2021**, *20*, 505–515.
12. Li, Y.; Ma, X.; Feng, N.; Shang, J.; Xu, X. Experimental Study on Seismic Response of Ji'nan Silty Clay and the Tunnel in It. *Chin. J. Undergr. Space Eng.* **2019**, *15*, 1652–1660.
13. Simoni, A.; Houlsby, G.T. The Direct Shear Strength and Dilatancy of Sand–gravel Mixtures. *Geotechn. Geol. Eng.* **2006**, *24*, 523–549. [CrossRef]
14. Huang, W. Large-Scale Triaxial Tests on Soil-Rock Aggregate Mixture Based on Orthogonal Design. Master's Thesis, Hunan University, Changsha, China, 2015.
15. Cao, W.G.; Huang, W.J.; Wang, J.Y.; Zhai, Y.C. Large-scale triaxial tests Study om Deformation and Intensity Characteristic of Soil-rock Aggregate Mixture. *J. Hunan Univ.* **2016**, *43*, 142–148.
16. Xia, J.; Hu, R.; Qi, S.; Gao, W.; Sui, H. Large-scale triaxial shear testing of soil rock mixtures containing oversized particles. *J. Rock Mech. Geotech. Eng.* **2017**, *36*, 2031–2039.
17. Xia, J.; Hu, R.; Gao, W. Research on Mechanical Characteristic of the Soil Rock Mixtures by Large-scale triaxial shear Tests. *J. Eng. Geol.* **2016**, *24*, 1211–1218.
18. Hu, S.; Jin, X.; Sun, G.; Li, H.; Nie, Z. Triaxial test and PFC-FLAC coupling simulation study on material parameters and deformation characteristics of soil-rock mixture. *J. Rock Mech. Geotech. Eng.* **2021**, *40*, 3344–3356. [CrossRef]